Saturation spectroscopy of iodine in hollow-core optical fiber

Anna Lurie,[1] **Philip S. Light,**[1] **James Anstie,**[1] **Thomas M. Stace,**[2] **Paul C. Abbott,**[1] **Fetah Benabid,**[3] **and Andre N. Luiten**[1,4,*]

[1]*School of Physics, The University of Western Australia, Crawley, Western Australia 6009, Australia*
[2]*Department of Physics, University of Queensland, Brisbane, Queensland 4072, Australia*
[3]*Centre for Photonics and Photonic Materials, Department of Physics, University of Bath, UK*
[4] *School of Physics and Chemistry, The University of Adelaide, Adelaide, South Australia, 5005 Australia*
[*]*Andre.Luiten@uwa.edu.au*

Abstract: We present high-resolution spectroscopy of I_2 vapor that is loaded and trapped within the core of a hollow-core photonic crystal fiber (HC-PCF). We compare the observed spectroscopic features to those observed in a conventional iodine cell and show that the saturation characteristics differ significantly. Despite the confined geometry it was still possible to obtain sub-Doppler features with a spectral width of ~ 6 MHz with very high contrast. We provide a simple theory which closely reproduces all the key observations of the experiment.

OCIS codes: (060.5295) Photonic crystal fibers; (300.6420) Spectroscopy, nonlinear; (300.6460) Spectroscopy, saturation.

References and links

1. J. Ye, L. Robertsson, S. Picard, M. Long-Sheng, and J. L. Hall, "Absolute frequency atlas of molecular I_2 lines at 532 nm," IEEE Trans. Instrum. Meas. **48**, 544–549 (1999).
2. J. Ye, L. S. Ma, and J. L. Hall, "Molecular iodine clock," Phys. Rev. Lett. **87**, 270801 (2001).
3. B. Argence, H. Halloin, O. Jeannin, P. Prat, O. Turazza, E. de Vismes, G. Auger, and E. Plagnol, "Molecular laser stabilization at low frequencies for the LISA mission," Phys. Rev. D **81**, 082002 (2010).
4. K. Nyholm, M. Merimaa, T. Ahola, and A. Lassila, "Frequency stabilization of a diode-pumped Nd:Yag laser at 532 nm to iodine by using third-harmonic technique," IEEE Trans. Instrum. Meas. **52**, 284-287 (2003).
5. G. D. Rovera, F. Ducos, J.-J. Zondy, O. Acef, J.-P. Wallerand, J. C. Knight, and P. St. J. Russell, "Absolute frequency meaurements of an I_2 stabilized Nd:YAG optical frequency standard," Meas. Sci. Technol. **13**, 918-922 (2002).
6. E. J. Zang, J. P. Cao, Y. Li, C. Y. Li, Y. K. Deng and C. Q. Gao, "Realization of four-pass I_2 absorption cell in 532-nm optical frequency standard," IEEE Trans. Instrum. Meas. **56**, 673–676 (2007).
7. F. Benabid, J. C. Knight, G. Antonopoulos, and P. St. J. Russell, "Stimulated Raman scattering in Hydrogen-filled hollow-core photonic crystal fiber," Science **298**, 399–402(2002).
8. F. Benabid, F. Couny, J. C. Knight, T. A. Birks, and P. St J. Russell, "Compact, stable and efficient all-fibre gas cells using hollow-core photonic crystal fibres," Nature **434**, 488–491 (2005).
9. V. Venkataraman, P. Londero, A. R. Bhagwat, A. D. Slepkov, and A. L. Gaeta, "All-optical modulation of four-wave mixing in an Rb-filled photonic bandgap fiber," Opt. Lett. **35**, 2287–2289 (2010).
10. S. Ghosh, J. E. Sharping, D. G. Ouzounov, and A. L. Gaeta, "Resonant optical interactions with molecules confined in photonic band-gap fibers," Phys. Rev. Lett. **94**, 093902 (2005).
11. J. Hald, J. C. Petersen, and J. Henningsen, "Saturated optical absorption by slow molecules in hollow-core photonic band-gap fibers," Phys. Rev. Lett. **98**, 213902 (2007).
12. P. S. Light, F. Benabid, F. Couny, M. Maric, and A. N. Luiten, "Electromagnetically induced transparency in Rubidium-filled HC-PCF PDMS coated hollow-core PCF," Opt. Lett. **32**, 1323–1325 (2007).
13. S. M. Hendrickson, M. M. Lai, T. B. Pittman, and J. D. Franson , "Observation of two-photon absorption at low power levels using tapered optical fibers in Rubidium vapor," Phys. Rev. Lett. **105**, 173602 (2010).

#164943 - $15.00 USD Received 19 Mar 2012; revised 18 Apr 2012; accepted 18 Apr 2012; published 10 May 2012

14. K. Knabe, S. Wu, J. Lim, K. A. Tillman, P. S. Light, F. Couny, N. Wheeler, R. Thapa, A. M. Jones, J. W. Nicholson, B. R. Washburn, F. Benabid, and Kristan L. Corwin, "10 kHz accuracy of an optical frequency reference based on $^{12}C_2H_2$-filled large-core kagome photonic crystal fibers," Opt. Express **17**, 16017–16026 (2009).
15. C. Perrella, P. S. Light, T. M. Stace, F. Benabid, and A. N. Luiten "High resolution optical spectroscopy in hollow core fibre," Phys. Rev. A **85**, 012518 (2012).
16. A. Lurie, F. N. Baynes, J. D. Anstie, P. S. Light, F. Benabid, T. M. Stace, and A. N. Luiten , "High-performance iodine fibre frequency standard," Opt. Lett. **36**, 4776–4778 (2011).
17. F. Couny, F. Benabid, and P. S. Light, "Large-pitch kagome-structured hollow-core photonic crystal fiber," Opt. Lett. **31**, 3574-3576 (2005).
18. W. Demtroder, *Laser Spectroscopy*, 3rd ed. (Springer, 2002).
19. G. Khitrova, P. R. Berman, and M. Sargent, "Theory of pump-probe spectroscopy," J. Opt. Soc. Am. B **5**, 160–170 (1988).
20. A. Schenzle and R. G. Brewer, "Optical coherent transients: Generalized two-level solutions," Phys. Rev. A **14**, 1756–1765 (1976).
21. M. A. Banash and W. S. Warren, "State-to-state collisional dynamics by coherent laser pulse phase, shape and frequency modulation," Laser Chem. **6**, 47–60 (1986).
22. T. S. Rose, W. L. Wilson, G. Wackerle, and M. D. Fayer, "Gas phase dynamics and spectroscopy probed with picosecond transient grating experiments," J. Chem. Phys. **86**, 5370–5391 (1987).
23. E. T. Sleva and A. H. Zewail, "Phase and energy-changing collisions in Iodine gas: studies by optical multiple-pulse spectroscopy," Chem. Phys. Lett. **110**, 582–587 (1984).
24. M. H. Ornstein and V. E. Derr, "Dye-laser scanning spectroscopy and fluorescence-quenching cross sections for the $B^3\Pi^+{}_{o,u}$, state of iodine," J. Opt. Soc. Am. **6**, 233–240 (1976).
25. S. V. Kireev and S. L. Shnyrev, "Rotational relaxation of the levels of the B State in ^{127}I and ^{129}I molecular Iodine isotopes excited by 633-nm radiation of a He–Ne Laser," Laser Phys. **9**, 614–625 (1999).
26. C. J. Bordé, J. L Hall, C. V. Kunasz, and D. G. Hummer, "Saturated absorption line shape: calculation of the transit-time broadening by a perturbation approach," Phys. Rev. A. **14**, 236–263 (1976).
27. G. A. Capelle and H. P. Broida, "Lifetimes and quenching cross sections of I_2 ($B^3\Pi_{Ou}{}^+$)," J. Chem. Phys. **58**, 4212–4222 (1973).
28. F.-L. Hong, Y. Zhang, J. Ishikawa, A. Onae, and H. Matsumoto, "Hyperfine structure and absolute frequency determination of the R(121)35-0 and P(142)37-0 transitions of $^{127}I_2$ near 532 nm," Opt. Commun. **212**, 89–95 (2002).
29. G. T. Phillips and G. P. Perram, "Pressure broadening by argon in the hyperfine resolved P(10) and P(70) (17,1) transitions of I_2 $X^1\Sigma(0_g{}^+) \rightarrow B^3\Pi(0_u{}^+)$ using sub-Doppler laser saturation spectroscopy," J. Quant. Spectrosc. Radiat. Transf. **109**, 1875–1885 (2008).
30. B. Hiller and R.K. Hanson, "Properties of the iodine molecule relevant to laser-induced fluorescence experiments in gas flows," Exp. Fluids **10**, 1–11 (1990).
31. H.-M. Fang, S. C. Wang, and J.-T. Shy, "Pressure and power broadening of the a10 component of R(56) 32-0 transition of molecular iodine at 532 nm," Opt. Commun. **257**, 76–83(2006) and references therein.
32. T. Maisello, N. Vulpanovici, and J. W. Nibler, "Fluorescence lifetime and quenching of Iodine vapor," J. Chem. Educ. **80**, 914–917 (2003).
33. C. Chardonnet, F. Guernet, G. Charton, and C. Bordé, "Ultrahigh-resolution saturation spectroscopy using slow molecules in an external cell," Appl. Phys. B **59**, 333–343 (1994).
34. D. G. Fletcher, and J. C. McDaniel, "Collisional shift and broadening of Iodine spectral lines in Ar near 543nm," J. Quant. Spectrosc. Radiat. Transfer **54**, 837–850, (1995).
35. M. Comstock, V. V. Lozovoy, and M. Dantusa, "Femtosecond photon echo measurements of electronic coherence relaxation between the $X(^1\Sigma_{g+})$ and $B(^3\Pi_{0u+})$ states of I_2 in the presence of He, Ar, N_2, O_2, C_3H_8," J. Chem. Phys. **119**, 6546–6553 (2003).
36. J. C. D. Brand and J. Hayward, "Determination of cross-sections for collisional energy transfer in the ground and excited states of I_2 by polarization spectroscopy," Chem. Phys. Lett. **68**, 369–373 (1979).

1. Introduction

Iodine vapor has played a prominent role in the frequency stabilization of lasers over many years because it exhibits a large number of intrinsically narrow spectral lines across a large fraction of the visible and near-IR spectrum. Some of the best performing vapor-cell frequency standards have used iodine in large-diameter (~ 10 cm) and long (~ 1 metre) vapor cells [1–6]. The large diameter minimizes broadening associated with transit of the molecules through the probing laser beam, while the long length allows operation at low pressures, thereby avoiding collisional broadening, while still demonstrating strong absorption features. In order to avoid the substantial challenges associated with using large and fragile vapor cells there has recently

#164943 - $15.00 USD Received 19 Mar 2012; revised 18 Apr 2012; accepted 18 Apr 2012; published 10 May 2012

been a great deal of research targeted towards loading vapors into the cores of specially tailored hollow-core photonic crystal fibre (HC-PCF). Although rubidium, ammonia and acetylene have all been loaded in the core of these fibers for both spectroscopic studies and frequency standards work [7–15], we are aware of just a single recent example of the use of iodine as a frequency standard [16], and no detailed examination of its spectra in this situation.

The key benefit of fiber technology is its robust and compact geometry, which lends itself to easy temperature control and magnetic-shielding, while still possessing the advantage of a long interaction zone (potentially even longer than the macroscopic glass cells). This long spatial interaction allows for strong absorption, which delivers a high signal to noise ratio, while simultaneously minimising the density of the molecules, and thereby the pressure broadening. Furthermore, for both spectroscopy and frequency-standards work, it is a common desire to circumvent Doppler broadening [3] effects. In this regard, the fiber approach offers a great advantage over cell-based techniques because it automatically ensures that there is a stable and effective overlap between the counter-propagating pump and probe lasers beams required for saturated absorption techniques. This high-quality overlap arises because the vapor is stored inside an optical waveguide. The experiments reported in this work demonstrate directly the quality of this overlap in the fibers. A further benefit of the iodine loaded HC-PCF for portable applications is that the guiding and confinement within the small core of the fiber allows high intensities over long lengths for a small power inputs, creating deep saturation features.

The most obvious drawback for fiber-based vapor cells is the limited duration of the coherent light-molecule interaction due to the small diameter of the fiber core. This limit causes an unavoidable line broadening (termed transit-time broadening) which is of the order of $\delta\omega_{TT} = v_{mp}/\phi$ where ϕ is the HC-PCF core diameter and v_{mp} the most probable velocity of the particles. The narrowest sub-Doppler bandwidths so far observed in HC-PCF have been in the range of 6-8 MHz [11, 12, 14, 15] and are limited by transit time broadening. Even to obtain these results it was necessary to use either a large core (70 μm) fiber [14], apply anti-relaxation coatings [12], or make use of velocity selection effects through careful excitation strategies [11, 15] to obtain narrow lines.

This work uses a different approach by making use of a large mass molecule to reduce v_{mp} for a given temperature gas. The mass of the $^{127}I_2$ molecule is ten times that of acetylene $^{12}C_2H_2$ and 15 times larger than ammonia NH_3 which gives a reduction in the potential transit time effects by a factor of 3-4 over those other vapors. This minimizes a key potential defect of fiber-based vapor cells.

In this paper we present iodine spectroscopy in the confined geometry of the hollow-core fiber and report, to our knowledge, the highest-Q spectral features yet observed in this environment. We compare these results to those from a conventional cell and illuminate some of the key differences. Further, we will present a relatively simple theoretical model which is in good agreement with the observed spectroscopic features.

2. Experiment

Iodine presents a dense spectra of ro-vibronic transitions ranging from green through to the near-IR part of the spectrum. Each of these transitions consists of either 15 or 21 hyperfine lines due to interaction with the two nuclear spins ($I = \frac{5}{2}$ for each nucleus). This hyperfine manifold is not properly resolved in the presence of Doppler broadening and thus in this experiment we made use of saturation spectroscopy to eliminate the inhomogeneous broadening. In order to enhance the signal to noise ratio of the weak sub-Doppler spectral features we use a particular variant of modulation-transfer spectroscopy (MTS) in which we amplitude modulate the pump and synchronously detect the resulting amplitude modulation on the probe signal.

A block diagram of the optical arrangement in shown in Fig. 1. The HC-PCF, manufactured

#164943 - $15.00 USD Received 19 Mar 2012; revised 18 Apr 2012; accepted 18 Apr 2012; published 10 May 2012

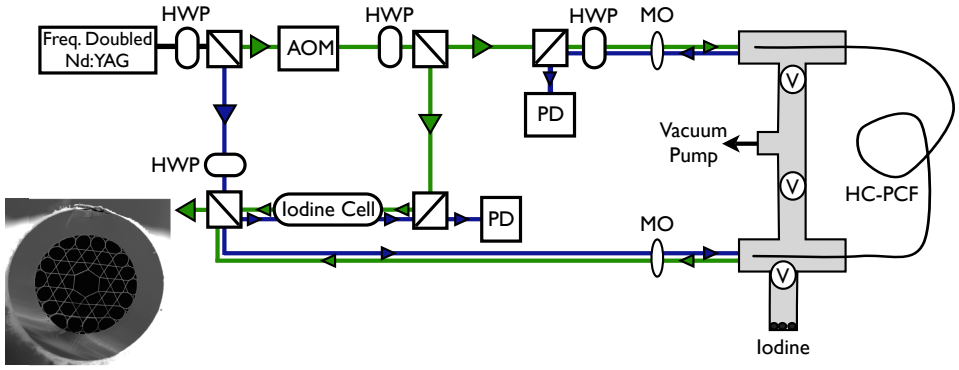

Fig. 1. Optical setup with counter-propagating pump (green) and probe (blue) beams. MO - microscope objective, AOM - acoustic optical modulator, PD - photodiode, HWP - half-wave plate, V - vacuum valves, with the counter-propagating beams separated for ease of visualization. The inset shows a micrograph of the fiber used in this experiment. The short and long axis diameters of the core are 23 and 27 μm respectively.

at the University of Bath [17], is mounted in a glass vacuum system with the majority of the 1.3 m fiber outside the vacuum. A micrograph of the kagome-type [17] cross-section of the HC-PCF is shown as an inset in Fig. 1. The fiber exhibits a loss of 0.7 dB/m at our operating wavelength. A Viton cone is used to produce a compressive seal between the fiber and glass at the two points where the fiber enters the vacuum system. The open end of the fiber is suspended inside the vacuum a few millimetres behind an optical window so that there is optical access to the core of the fiber during the filling phase. Light is coupled into each end of the fiber using a 4$\times$ microscope objective mounted on a three-axis translation stage. We obtain a total transmission, including fiber input and output coupling losses as well as attenuation due to the fiber and the gas chamber window, of around 60%. Solid iodine is kept in a separate section of the vacuum system at room temperature (equilibrium vapor pressure 36$\pm$1 Pa) and is released into the HC-PCF after the vacuum system has been evacuated down to a pressure of 8×10^{-4} Pa. The vacuum valves consist of a glass housing with a teflon valve body as this was found to minimize unwanted chemical interactions with the iodine vapor.

A narrow-linewidth frequency-doubled Nd:YAG laser provides 20 mW of 532 nm laser light that is tunable over $\sim$60 GHz by controlling the crystal's temperature. This output light is split and counter-propagating pump and probe beams are sent through both the iodine-filled fiber and a 10 cm long traditional iodine gas cell (vapor pressure 36$\pm$1 Pa, probe beam diameter $\sim$ 250 μm, pump beam diameter $\sim$ 470 μm) operated concurrently as a reference. The transmitted probe light is separated from reflected pump light, using a polarizing beam-splitter and careful polarization tuning, and then sent to a monitoring photodetector. Despite this care, scattered pump light still caused interference on the detector - to overcome this the pump light was shifted by 200 MHz using an Acousto-Optical Modulator (AOM). This same AOM provided the amplitude modulation necessary for the MTS technique with 100% modulation depth at a 9.2 kHz rate. The output voltage of the photodiode was monitored by two instruments as the laser frequency was slowly swept: (i) the average voltage was measured to provide an estimate of the conventional linear absorption of iodine, (ii) the probe amplitude modulation transferred from the pump modulation was demodulated with a lock-in amplifier to measure the magnitude of the sub-Doppler features.

#164943 - $15.00 USD Received 19 Mar 2012; revised 18 Apr 2012; accepted 18 Apr 2012; published 10 May 2012

3. Theory

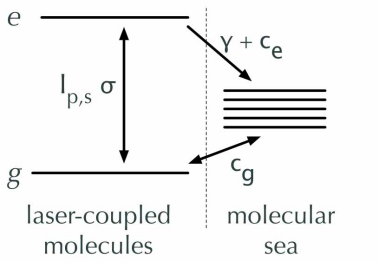

Fig. 2. Schematic plot of the "open" two-level model of iodine molecules used in the theory presented here. Counter-propagating laser light of power $I_{p,s}$ drives stimulated transitions between the ground, g, and excited, e, states. Collisions with molecules in the ground and excited states (at rates c_g and c_e respectively) exchange molecules between the laser-coupled and uncoupled states.

We use a simple "open" two level rate-equation model to describe the saturation spectroscopy of iodine (see Fig. 2) [18,19]. This rate-equation approach is valid because the high rate of collisions keep the atomic coherences small (adiabatic approximation). We include in our rate equations collisional processes that knock the molecules out of resonance with the laser light - either because their velocity has been changed or because their rotational, vibration or electronic state is modified. In either case the molecules are considered to return to a large "sea" of non-interacting iodine molecules [20–22]. We note the close agreement between theory and experiment which would appear to lend credence to this approach.

We define rate equations for the excited ($e(t)$) and ground ($g(t)$) states in the reference frame of the molecule and imagine it to be interacting with two different colour laser signals representing a probe beam (labelled with "s" subscript) and a counter-propagating pump (labelled with "p" subscript):

$$\dot{e}(t) = \frac{(g-e)I_p\sigma}{1+\frac{{\delta_p}^2}{(w_0/2)^2}} + \frac{(g-e)I_s\sigma}{1+\frac{{\delta_s}^2}{(w_0/2)^2}} - e(c_e+\gamma) \tag{1}$$

$$\dot{g}(t) = (\rho\,[\delta_v]-g)c_g - \frac{(g-e)I_p\sigma}{1+\frac{{\delta_p}^2}{(w_0/2)^2}} - \frac{(g-e)I_s\sigma}{1+\frac{{\delta_s}^2}{(w_0/2)^2}} \tag{2}$$

where $\delta_p = \delta_a - (\delta_{AOM} + \delta_l + \delta_v)$ and $\delta_s = \delta_a - (\delta_l - \delta_v)$ represent the pump and probe laser detunings from the molecular resonance frequency, δ_a, translated into the frame of a molecule moving at a velocity $v = \delta_v/k$. δ_{AOM} takes account of the the fixed AOM frequency which detunes the laser frequency, δ_l in the pump arm. We include different collisional rates for the excited (c_e) and ground state (c_g) because the effect of collisions on the iodine molecule has been shown to be highly state-dependent and collision-partner dependent [20,21,23–25]. We include a population loss rate for spontaneous emission from the excited state (γ) although, due to the multitude of possible decay routes, we have not included a corresponding gain in the ground state due to this process [18]. On the other hand we have included a gain term ($\rho\,[\delta_v]\,c_g$) in the ground state representing scattering from a "sea" of uncoupled states into the laser-coupled ground state. The inhomogenous broadening is contained in the velocity detuning dependence of the $\rho\,[\delta_v]$ term. The pumping rates $I_{p,s}$ are given in terms of a photon rate per area while the scattering cross-section, σ (units m^2), is defined such that $\sigma I_{p,s}$ is the on-resonance photon scattering rate from a molecule irradiated with an intensity $I_{p,s}$ on the particular transition of

#164943 - $15.00 USD Received 19 Mar 2012; revised 18 Apr 2012; accepted 18 Apr 2012; published 10 May 2012

interest. All relaxation and pumping rates are expressed in units of s^{-1}, while all frequencies are expressed in angular frequency units.

The homogenous bandwidth of the molecule-light interaction, w_0, is set by the total coherent interaction time. Where the probe and pump beams are sufficiently large in diameter that transit-time broadening is not a consideration (e.g. in the conventional free-space cell experiment), the bandwidth will be $w_0 = c_e + c_g + \gamma$. However, when transit-time effects are significant (as with the fiber experiment) then the homogeneous bandwidth is calculated using the formalism in Ref. [26]. The early termination of the interaction between the probe light and molecules due to its complete transit is modelled in the rate equations with an additional effective collision that adds equally to both c_e and c_g (since it terminates the light interaction whether we are in the ground or excited states). In our experimental conditions, the natural lifetime [27] of the upper state ($1/\gamma \sim 1\mu$s) is substantially longer than the mean time between collisions for the excited state ($c_e > \gamma$) and so can usually be ignored.

We calculate the absorption of the probe based on energy lost from the excited state through collisions or spontaneous emission i.e. energy lost per unit time and volume will be $e_s \times (c_e + \gamma)h\nu$, where e_s is restricted to that fraction of the excited state that has been produced by the probe alone. We use the usual relations to connect the scattered energy to the absorption coefficient [18].

The rate equations are solved in the steady-state ($\dot{e}(t) = 0, \dot{g}(t) = 0$) to obtain relationships between the model and the experimentally observable features: absorption, saturation intensity and the height and width of the Doppler-free features. The intensity dependence of the on-resonance ($\delta_s = 0$) probe absorption can be calculated by setting the pump intensity to zero ($I_p = 0$) and integrating the steady-state solutions over the Doppler broadening implicitly contained in $\rho\,[\delta_a]$ to obtain:

$$\alpha_D = \rho_0 \sigma \left(1 + \frac{I_s}{I_{\text{sat}}}\right)^{-1/2} \tag{3}$$

where $\rho_0 = \frac{\rho[\delta_a]\pi w_0}{2}$ is the population spectral density integrated over the homogeneous bandwidth, and we interpret I_{sat} as $\frac{(c_e+\gamma)c_g}{\sigma(c_e+\gamma+c_g)} \sim \frac{c_e c_g}{\sigma(c_e+c_g)}$ as the saturation rate for the linear absorption. Importantly for our analysis below we note that if there is a large disparity between the ground and excited state collisional rates then the saturation rate will equal the slower of the two rates. In contrast, the bandwidth, w_0, is equal to the sum of the collisional rates and hence will be approximately equal to the larger of the two collisional rates in that situation. This different dependence of the bandwidth and saturation intensity allows us to understand a key observed difference in the spectroscopic observations of the fiber and cell experiments.

In the presence of the pump one sees a narrow feature in the probe absorption arising out of the modifications of the ground and excited state populations by the pump. This feature is centred on $\delta_p = \delta_s$ (or equivalently $\delta_l = \delta_a - \delta_{AOM}/2$). For $I_p, I_s < 100 I_{\text{sat}}$ this feature closely follows a Lorentzian shape: $\mathscr{L}(\delta) = A/(1 + 4\delta^2/w^2)$. The probe absorption observed far from this narrow feature is self-evidently equal to that calculated in Eq. 3 since the pump and signals do not interact when tuned to different velocity classes. In the limit that the probe is not self-saturating, the effective saturation dip contrast (ratio of the the saturation feature height to the linear absorption) will be:

$$C = 1 - \frac{1 + I_p/(2I_{\text{sat}})}{(1 + I_p/I_{\text{sat}})^{3/2}} \tag{4}$$

One sees that the contrast reaches $\sim 50\%$ for $I_p \sim I_{\text{sat}}$. The final key element of interest is the bandwidth of the saturation feature. We find that there is no simple closed-form expression for

#164943 - $15.00 USD Received 19 Mar 2012; revised 18 Apr 2012; accepted 18 Apr 2012; published 10 May 2012

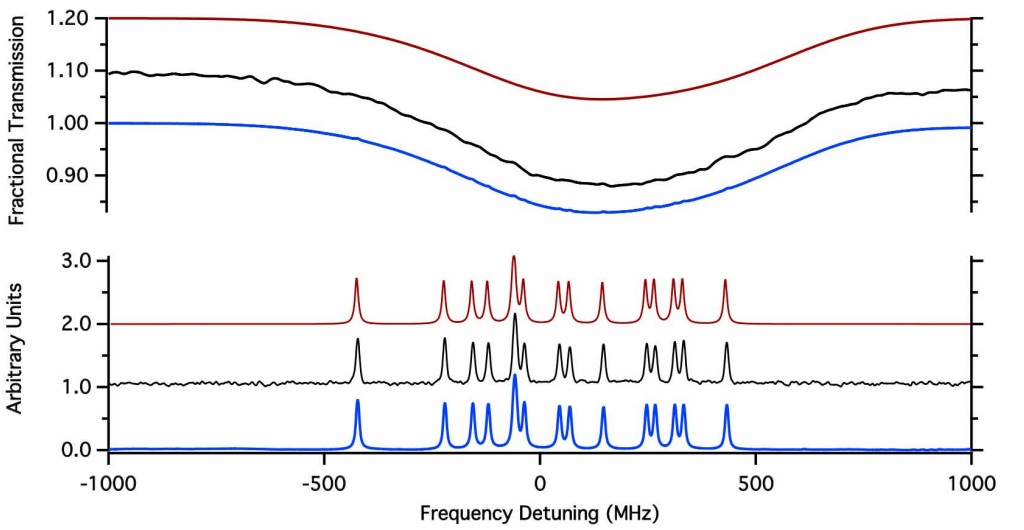

Fig. 3. The P(142)37-0 Doppler-broadened (upper panel) and Doppler-free spectrum (lower panel) recorded in the cell (lowest traces- blue), in the fiber (middle traces -black) and calculated using the theory presented in Sect. 3 (highest traces - red). For the experiment the pump intensity was 41 kWm^{-2} and 25 kWm^{-2} for the fiber and cell respectively with probe intensities less than 20% of that of the pump. For the theory, we have used $w_0 = 6$ MHz; $\rho_0\sigma = 0.02$; $I_p/I_{sat} = 1$ (to nearly match the cell conditions) and summed the response of all 15 hyperfine features using the known frequency spacings in Ref. [28]. We have normalized the frequency axis to the centre of mass of the transition at 563.281 THz [28]. The a1 hyperfine component is the lowest frequency component in the hyperfine spectrum near -424 MHz and is 28% and 8% of the height of the Doppler absorption of the cell and fibre respectively. For clarity the lower traces have been offset by 1 unit, while the upper traces are offset by 0.1 units.

this although the expression below is within 1% of the correct value over all realistic pump power values ($I_p < 100 I_{\mathrm{sat}}$):

$$w = w_0\sqrt{1 + I_p/(\sqrt{2}I_{\mathrm{sat}})} \tag{5}$$

As expected the low power bandwidth equals w_0 while additional broadening is seen as the pump power exceeds I_{sat}.

4. Results

Figure 3 shows the linear and sub-Doppler absorption spectra for the P(142) 37-0 iodine transition in the cell (10 cm long) and fiber (1.3 m) respectively using similar pump intensities. This is close to the maximum available intensity in the cell and near to the minimum used in the fiber case (because of poor signal to noise at these low power levels). The additional noise seen on the fiber data comes because the power is 600 times below that used in the cell along with some vibrational noise which modulated the power coupled into the fiber core. The SNR (measurement bandwidth of 1kHz) was 70 and 20 for the cell and fibre respectively. From this figure it is evident that both measurements give extremely similar characteristics for the sub-Doppler features despite the confined geometry within the fiber core.

As can be seen on Fig. 3 both the fiber and cell have a maximum linear absorption of around

#164943 - $15.00 USD Received 19 Mar 2012; revised 18 Apr 2012; accepted 18 Apr 2012; published 10 May 2012

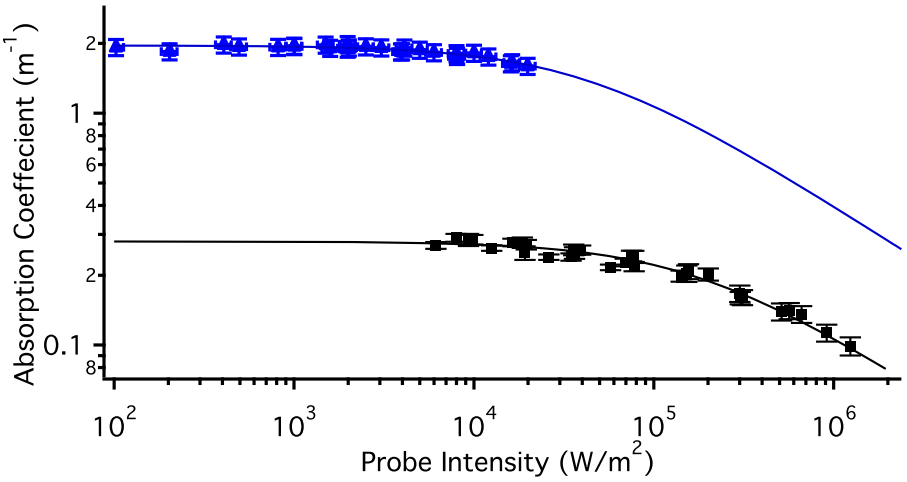

Fig. 4. Linear Absorption of the P(142) 37-0 line as a function of probe intensity. Black markers show measurements from fiber measurement while the blue markers show measurements from cell. Solid curves in both cases are fits following the form of Eq. 3. It is evident that the number density of the cell and fiber differ substantial as do the saturation intensities.

20% on resonance. The particular shape of the Doppler-broadened curve arises because it is the sum of 15 underlying hyperfine components each of which is broadened by the FWHM Doppler width of 437 MHz for iodine at room temperature. In light of the small linear absorption we have made no allowance for axial variation in intensity in our model. Our total end-to-end transmission loss through the fiber is around 60% of which 20% is associated with the separately measured fiber attenuation (1.3 m, 0.7 dB/m). The rest of the loss is attributed to input coupling losses associated with mode-matching inefficiencies. For laser intensities quoted for the optical fiber experiments we have corrected the measured input intensities by a factor of 1.5 to allow for the input loss.

4.1. Linear absorption

We recorded a large number of spectra of the type shown on Fig. 3 for both cell and fiber where as the pump or probe intensity was varied. We used the known frequency spacing between the a1 and a15 hyperfine components (855 MHz [28]) to provide a frequency axis for these measurements. From these spectra we derived the on-resonance absorption coefficient together with the contrast and bandwidth of the Doppler-free features as a function of intensity. Below we will examine each of these measurements and compare them to the theoretically expected result.

Figure 4 presents the absorption coefficient for the cell and fiber as a function of the probe intensity. The ratio of the low power absorption coefficients is ~ 0.15 and if we combine this with the known equilibrium vapor pressure of iodine at room temperature in the cell then we can calculate the vapor pressure in this particular fiber load at around 5.4 ± 0.8 Pa. The solid lines shown on Fig. 4 are a fit using Eq. 3 and from this we extract a saturation intensity of 42 ± 4 kW/m^2 and 168 ± 14 kW/m^2 for the cell and fiber respectively. This result indicates that the effective collisional rate, $\frac{c_e c_g}{(c_e + c_g)}$, must differ substantially between the fiber and cell in spite of the similar decoherence rates in the two cases (see Fig 3 which shows that bandwidths are

#164943 - $15.00 USD Received 19 Mar 2012; revised 18 Apr 2012; accepted 18 Apr 2012; published 10 May 2012

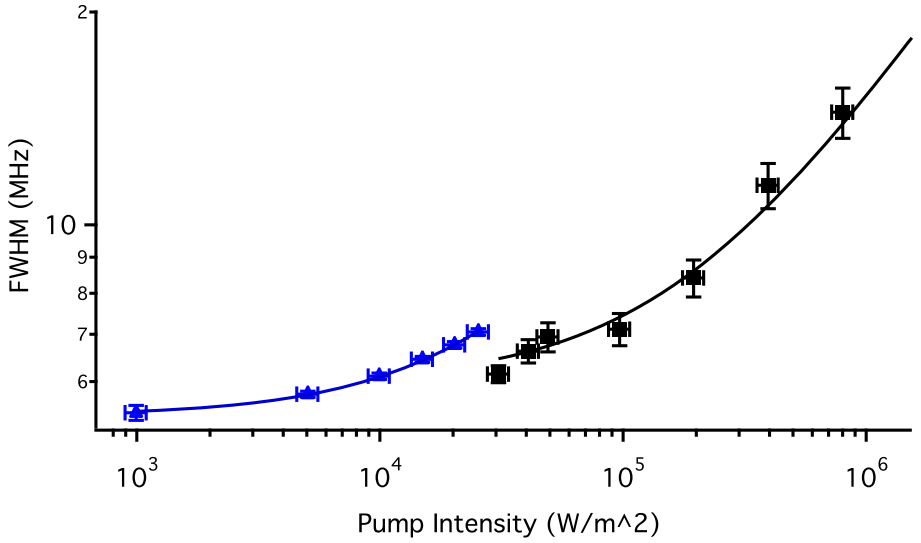

Fig. 5. The dependence of the bandwidth (FWHM) of the a1 component of the P(142) 37-0 iodine transition on pump power. We examine a 10cm long traditional glass iodine cell (blue markers), and the iodine loaded HC-PCF (black markers). Solid curves in the two cases are fits to the data following the form of Eq. 5.

around the same).

4.2. Sub-Doppler feature bandwidth

To further emphasise this point, we examine the bandwidth of the sub-Doppler features seen on the lower panel of Fig. 3 over a range of different pump powers. We fit a Lorentzian function to the a1 component in each trace and have summarised these measurements on Fig. 5. We also present on this figure solid curves of the form of Eq. 5, which can be seen to be in close agreement with the experiment. The fits yield nearly near-identical "zero-intensity" bandwidths of 5.40 ± 0.02 MHz for the cell and 6.0 ± 0.3 MHz in the fiber. On the other hand, the saturation intensities for the two cases are once again quite disparate giving pump beam saturation intensities of $I_{sat} = 24.0 \pm 0.5\,\mathrm{kWm}^{-2}$ and $I_{sat} = 129 \pm 16\,\mathrm{kWm}^{-2}$ respectively. In order to obtain high signal to noise features the probe intensity was around 40% of the pump intensity for this data which caused some unwanted broadening by the probe itself. If we examine the data as a function of total intensity instead of pump intensity we find cell and fibre saturating intensities of $I_{sat} = 33.6 \pm 0.5\,\mathrm{kWm}^{-2}$ and $I_{sat} = 181 \pm 16\,\mathrm{kWm}^{-2}$ respectively. These numbers are in agreement with those found from the linear absorption measurements to within 20%. We believe the residual disagreement comes from intensity calibration and fiber coupling variations.

The fact that the "zero-intensity" bandwidths are almost identical in the cell and fiber indicates that the total de-phasing rates are similar; however, the saturation intensity is seen to be very different (~ 5 times higher in the fiber than the cell). We believe that the origin of this apparent paradox lies in the fact that the ratio c_g/c_e differs substantially for the fiber and the cell.

4.3. Origins of feature bandwidth in fiber and cell

In the cell, the low-intensity bandwidth arises from collisional broadening effects since transit-time broadening and lifetime broadening are negligible in comparison. The dominant broad-

#164943 - $15.00 USD Received 19 Mar 2012; revised 18 Apr 2012; accepted 18 Apr 2012; published 10 May 2012

ening process in the cell is from iodine-iodine collisions (self-broadening). Although there is a high degree of variation (more than a factor of 2) in the literature values for the broadening coefficients for various transitions, our measurement falls within the range of previously measured values [29–32]. In the fiber, the iodine pressure is only 15% of that of the cell (from the linear absorption coefficient measurement at low intensities), which leads to an expected collisional self-broadening of just 0.8 MHz, which is in contradiction with the measured value of 6 MHz. However, in the fiber we expect an additional broadening process arising from the transit of the molecules across the narrow optical mode. The total bandwidth arising from these combined broadening processes depends upon the regime of observation, which is categorised by the dimensionless parameters [11,26,33]: $\eta = \Gamma r/v$ and $\theta = \Omega r/v = \sqrt{I_p/(2I_{sat})}\eta$, where r is the probe beam of 1/e radius, and v is the most probable thermal velocity. η can be thought to represent the number of collisions that occur in a typical beam crossing time, while θ is the number of Rabi cycles that occur in a typical beam crossing time. For our "zero-intensity" bandwidth measurement $\theta \ll 1$ and $\eta \sim 0.3$ ($\Gamma \sim 0.8\,MHz, r \sim 9\mu$m, $v \sim 139\,\mathrm{ms}^{-1}$). The predicted bandwidth [11, 26, 33] (full-width at half maximum) in this regime is given by $w_0 = 0.48\eta^{0.5}v/r \sim 4.2$ MHz, while the experimental measurement is just ~ 1.8 MHz larger than this. We believe that the origin of this small additional contribution to the bandwidth, which corresponds to just 0.8 MHz of additional collisional broadening, comes from background gas molecules (water/nitrogen/oxygen) that are loaded into the fiber along with the iodine. Lending support to this conjecture is an observed slow increase in the measured bandwidth ($\sim 7\%$ per hour) after the loading process. This unwanted background is associated with the poor pumping efficiency enforced by the unfortunate aspect ratio of the optical fiber core together with the use of teflon and Viton in the rest of the vacuum system, which prevents an effective pre-baking of the vacuum system. Assuming this background gas to be mainly air we estimate a background pressure of approximately 17 Pa [34, 35]. If it were possible to eliminate this background gas using an improved vacuum apparatus, while also reducing the iodine pressure by a factor of 5, then it should be possible to obtain a feature bandwidth of just ~ 2.6 MHz limited mostly by transit-time broadening with a small residual collisional component [26]. A fiber of ~ 5 m would yield similarly strong absorption features as those reported here.

We note that the termination of coherent light interaction by the transit-time effect is a state-independent process that will add equally to the effective collision rates for the excited and ground state. Similiarly, collisions with background gas atoms (in contrast to iodine-iodine collisions) show very similar collisional cross-sections for both excited and ground state collisions [36]. These facts suggest that for the fiber, with its small diameter mode and background gas contamination, we might expect $c_g \sim c_e$. On the other hand, iodine-iodine collisions produce a high degree of quenching and perturbation to the excited state molecules, while leaving ground state molecules relatively unperturbed i.e $c_g < c_e$ for a iodine-iodine collision [21, 24, 30]. We believe that these effects explain the factor of 5 difference between the saturation intensity of the fiber and cell in spite of the total dephasing rates being similar for the two cases. If $c_{e,\mathrm{cell}}/c_{g,\mathrm{cell}} \sim 0.2c_{e,\mathrm{fiber}}/c_{g,\mathrm{fiber}}$ then we would expect an $I_{sat,\mathrm{cell}} \sim 0.2I_{sat,\mathrm{fiber}}$ in accord with our results. In different words, the low rate of population decay from the molecular ground state in the cell (due to the long lifetime of this state when iodine-iodine collisions are dominant [21]) leads to a bottleneck in the interchange of laser-coupled molecules with the background sea. This leads to a media that is much more easily saturated when compared to the fiber.

4.4. Sub-Doppler feature contrast

To provide further confirmation of our understanding of the system we can examine the effect of pump intensity on the contrast of the P(142)37-0 a1 saturation feature (as per Eq. 4).Within a

#164943 - $15.00 USD Received 19 Mar 2012; revised 18 Apr 2012; accepted 18 Apr 2012; published 10 May 2012

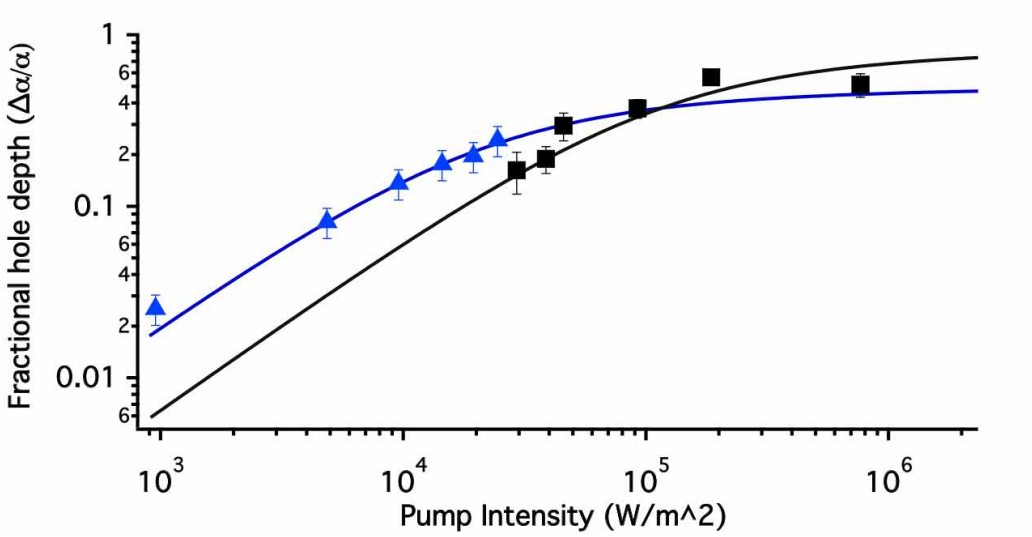

Fig. 6. The contrast of the a1 component of the P142(37-0) line as a function of pump intensity. The blue triangles show data from the cell, while the black squares show data from the fiber experiment. The probe intensity was maintained at $\sim$ 20% of the pump in both cases. The solid lines show fits of the form $C\,k_{\mathrm{eff}}$ where C comes from Eq. 4. We have held I_{sat} constant at the value derived from Fig. 5 and the only free parameter is k_{eff}.

single Doppler-broadened transition (see Fig. 3) there are a manifold of possible transitions (15 hyperfine levels in this case), and each of these other components contributes to the Doppler-broadened absorption at the location of the a1 hyperfine component. This overlap acts to reduce the apparent contrast of the feature with respect to the Doppler background. In order to make a meaningful comparison between theory and experiment we calculated the influence of the other hyperfine components at the location of the a1 component and corrected the measured contrast for this factor. A numerical calculation using the known spacings and relative strengths of the hyperfine components [28] results in a correction to the measured contrast of a factor of 1.78.

Figure 6 shows the measured contrast with the corrective factor applied. The solid lines on this figure are of the form $C\,k_{\mathrm{eff}}$ where C is derived from Eq. 4. We have included k_{eff} to express any imperfections to the beam overlap between pump and probe, which would act to prevent the contrast from reaching unity at the highest pump powers. This imperfect overlap can arise from attenuation of the pump and probe beams due to absorption through the vapor, or by fiber attenuation, or through poor alignment of the pump and probe beams. We have held the saturation intensities fixed at those derived from the bandwidth data shown on Fig 5 and only allowed k_{eff} to vary to generate the fits shown as solid lines on Fig. 6. The overlap efficiency, k_{eff}, was found to be 48% for the cell data, while it is around 82% for the fiber data, thereby demonstrating the improved mode-matching of the pump and probe beams in the fiber.

5. Conclusion

This paper has demonstrated loading of a hollow-core fiber with $^{127}I_2$. We have presented Doppler-free and Doppler-broadened spectroscopic measurements on a particular iodine transition at 532 nm (P(142) 37-0). At room temperature, the a1 hyperfine component of this transition shows a low power bandwidth of 6 MHz in the HC-PCF. The bandwidth observed in this confined geometry compares favourably to the narrowest bandwidths measured for acetylene

#164943 - $15.00 USD Received 19 Mar 2012; revised 18 Apr 2012; accepted 18 Apr 2012; published 10 May 2012

vapor in HC-PCF [11] and of rubidium [15]. We have shown that the current bandwidth is limited by collisions with background gas atoms and predict that by improving the vacuum and iodine loading system we could achieve bandwidths below 3 MHz. We have shown that the the fiber approach leads to an excellent efficiency for saturated absorption spectroscopy because of the high mode-overlap between the required pump and probe beams. The Q-factor for this transition is 9×10^7, which we believe to be the highest ever observed in hollow-core fiber.

Acknowledgments

The UWA authors would like to thank the Australian Research Council for supporting this research through DP0877938 and FT0990301 research grants. We would like to thank Chris Perrella and Gar-Wing Truong for insightful remarks on the manuscript and the rest of the group for creating a stimulating environment. Finally, we would like to thank Jan Hall for his highly useful contributions in the early stages of this project.

#164943 - $15.00 USD Received 19 Mar 2012; revised 18 Apr 2012; accepted 18 Apr 2012; published 10 May 2012